Molecular Therapy
Nucleic Acids
Original Article

Alleviation of ischemia-reperfusion induced renal injury by chemically modified *SOD2* mRNA delivered via lipid nanoparticles

Yutong Hou,[1,8] Sihao Lin,[2,8] Jia Xia,[3,8] Yu Zhang,[1] Yanan Yin,[1] Masha Huang,[1] Yingjie Xu,[1,4,5,7] Wen Yang,[1,6] and Yingjian Zhu[2]

[1]Department of Biochemistry and Molecular Cell Biology, Shanghai Key Laboratory for Tumor Microenvironment and Inflammation, Shanghai Jiao Tong University School of Medicine, Shanghai 200025, P.R. China; [2]Department of Urology, Jiading Branch of Shanghai General Hospital, Shanghai Jiao Tong University School of Medicine, Shanghai 201803, P.R. China; [3]Department of Nephrology, Renji Hospital, Shanghai Jiao Tong University School of Medicine, Shanghai 200127, P.R. China; [4]Key Laboratory of Cell Differentiation and Apoptosis of Chinese Ministry of Education, Shanghai Jiao Tong University School of Medicine, Shanghai 200025, P.R. China; [5]RNAcure Biopharma, Shanghai, P.R. China; [6]State Key Laboratory of Oncogenes and Related Genes, Shanghai, P.R. China; [7]Shanghai Frontiers Science Center of Cellular Homeostasis and Human Diseases, Shanghai, P.R. China

Ischemia-reperfusion injury (IRI) is a major cause of acute kidney injury, which is a serious clinical condition with no effective pharmacological treatment. Mesenchymal stem cell-derived extracellular vesicles (MSC-EVs) significantly alleviate kidney IRI; however, the underlying mechanisms and key molecules conferring renoprotection remain elusive. In this study, we characterized the protein composition of MSC-EVs using a proteomics approach and found that mitochondrial protein superoxide dismutase 2 (SOD2) was enriched in MSC-EVs. Using lipid nanoparticles (LNP), we successfully delivered chemically modified *SOD2* mRNA into kidney cells and mice with kidney IRI. We demonstrated that *SOD2* mRNA-LNP treatment decreased cellular reactive oxygen species (ROS) in cultured cells and ameliorated renal damage in IRI mice, as indicated by reduced levels of serum creatinine and restored tissue integrity compared with the control mRNA-LNP-injected group. Thus, the modulation of mitochondrial ROS levels through SOD2 upregulation by *SOD2* mRNA-LNP delivery could be a novel therapeutic method for ischemia-reperfusion-induced acute kidney injury.

INTRODUCTION

Ischemia-reperfusion (IR)-induced acute kidney injury (AKI) is a relatively common but severe pathological condition characterized by interrupted blood supply to the kidneys, followed by restoration of blood flow and reoxygenation.[1] IR-induced AKI contributes to high mortality and morbidity levels and induces rapid dysfunction in the kidney and other distant organs, including the liver, heart, and lung.[2] Recent studies have emphasized the importance of mitochondrial malfunction, including fragmentation, reduced biogenesis, reduced ATP production, and increased oxidative stress during reperfusion, in the pathophysiology of IR-induced AKI, which is not yet fully understood.[3–5] Hypoxia and reperfusion generate reactive oxygen species (ROS) that initiate a dynamic deleterious cellular response leading to an inflammatory cascade, cell death, and subsequent renal failure.[6] Other inflammatory mediators, including cytokines, adhesion molecules, chemokines, and pathological pathways such as leukocyte activation, are also involved in the process of IR-induced AKI.[7,8]

IR-induced AKI poses a critical clinical challenge because no medications currently exist for preventing or treating this condition that have proven clinical efficacy and safety. In the ischemia-reperfusion injury (IRI) mouse model, mesenchymal stem cell (MSC)-derived extracellular vesicles (MSC-EVs) have been shown to ameliorate tissue damage, reduce inflammation and oxidative stress, and promote renal functional recovery after IRI.[9,10] Extracellular vesicles (EVs) are small membrane vesicles released into the extracellular space upon fusion of multivesicular bodies with the plasma membrane. EVs carry a complex cargo of proteins,[11] lipids,[12] and genetic material,[13,14] and play an important role in intercellular communication by delivering these bioactive materials to surrounding or distal recipient cells. Although MSC-EVs exhibit advantages as effective biocarriers, several potential challenges limit their clinical application, such as difficulty obtaining

Received 21 March 2023; accepted 24 October 2023;
https://doi.org/10.1016/j.omtn.2023.102067.

[8]These authors contributed equally

Correspondence: Yingjie Xu, Department of Biochemistry and Molecular Cell Biology, Shanghai Key Laboratory for Tumor Microenvironment and Inflammation, Shanghai Jiao Tong University School of Medicine, Shanghai 200025, P.R. China.
E-mail: xuyingjie@shsmu.edu.cn
Correspondence: Wen Yang, Department of Biochemistry and Molecular Cell Biology, Shanghai Key Laboratory for Tumor Microenvironment and Inflammation, Shanghai Jiao Tong University School of Medicine, Shanghai 200025, P.R. China.
E-mail: yangwen@shsmu.edu.cn
Correspondence: Yingjian Zhu, Department of Urology, Jiading Branch of Shanghai General Hospital, Shanghai Jiao Tong University School of Medicine, Shanghai 201803, P.R. China.
E-mail: zhuyingjian_sjtu@126.com

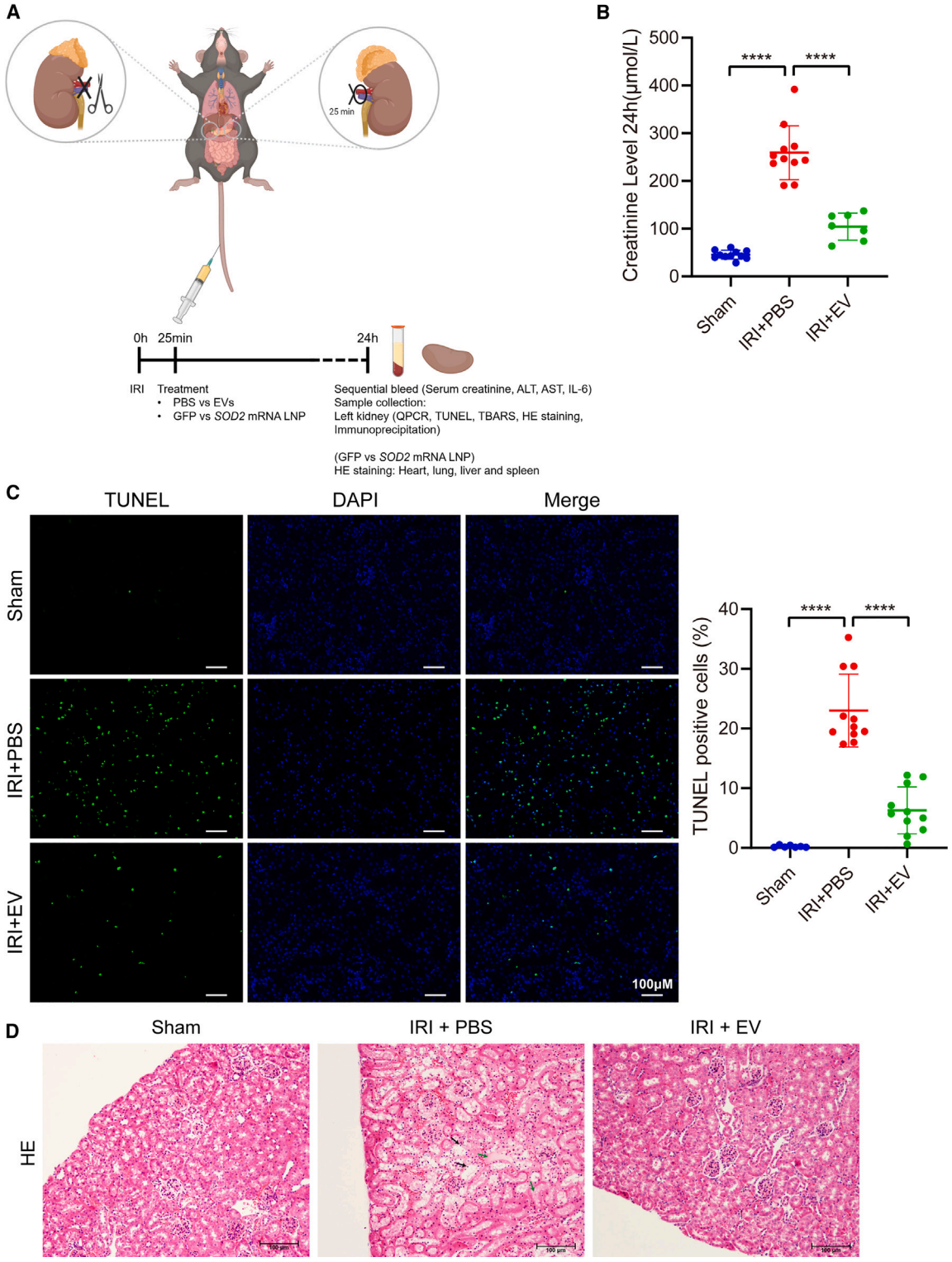

Figure 1. MSC-EVs reduced ischemia-reperfusion-induced renal injury

(A) Outline of animal experiments and schematic diagram of the acute kidney injury model: C57BL/6J mice were anesthetized and the ischemia-reperfusion model was performed by clamping renal vessels for 25 min while the other side of the kidney was removed. Mesenchymal stem cell (MSC)-derived extracellular vesicles (MSC-EVs)/

(legend continued on next page)

high amounts of pure exosomes.[15] Moreover, the key components in EVs and the underlying mechanisms controlling their renoprotective effect are not well defined.

During IRI, the generation of large amounts of ROS results in progressive functional deterioration of mitochondria, which leads to renal tissue injury via the peroxidation of membrane lipids and cell death via the oxidative damage of proteins and DNA.[16] Therefore, the inhibition or prevention of oxidative stress may protect tissues from IR-induced damage. Several approaches have exhibited beneficial antioxidative properties in IRI, such as antioxidant agents and free radical scavengers.[17–21] In addition, the downregulation of antioxidant enzymes, such as superoxide dismutase (SOD), glutathione peroxidase, and catalase, has been observed during IR,[22] suggesting that restoration of these enzymes may be a straightforward way to reduce ROS levels and oxidative stress, and consequently prevent IRI.

Lipid nanoparticle (LNP) delivery of small interfering RNA and mRNA has recently been approved as a powerful therapeutic strategy for a wide range of clinical applications. *In vitro*-transcribed (IVT) mRNA, which is structurally similar to the mature and processed mRNA of eukaryotic cells, provides genetic information that enables the translation machinery of the host cell to produce encoded target proteins.[23] These proteins can act as antigens to stimulate the immune response or supplement functionally beneficial proteins.[24,25] Moreover, IVT-mRNA has the following advantages: no risk of genomic integration, fast and predictable protein expression kinetics, and natural degradation products.[26] More importantly, the use of various chemical modifications not only reduces the immunogenicity of IVT-mRNA,[27] but also enhances mRNA stability and translation efficiency, while safe and effective delivery platforms such as LNP can encapsulate mRNA and ensure its *in vivo* uptake and expression.[28] Thus, mRNA is currently a promising therapy in the fields of vaccine development for both infectious diseases and cancer, protein replacement therapy, and genome engineering for the treatment of rare diseases.

In this study, we determine the mitochondrial component inside MSC-EVs and identify the antioxidant enzyme superoxide dismutase 2 (SOD2) as one of the most abundant proteins by proteomics analysis. We then demonstrate that the delivery of chemically modified *SOD2* mRNA via LNP alleviates kidney IRI in mice.

RESULTS

Protective effect of MSC-EVs in ischemic AKI *in vivo*

To examine the function of MSC-EVs *in vivo*, we first obtained EVs from the MSC culture supernatant. Transmission electron microscopy of negatively stained EVs revealed cup-shaped particles (Figure S1A), indicating an intact bilipid membranous vesicle. We performed western blot analysis on EVs. As expected, EVs were positive for classical EV markers such as CD63, CD81, Alix, and TSG101 (Figure S1B). We then established an IR-induced renal injury mouse model to examine the therapeutic effect of MSC-EVs. In this model, the left renal pedicle was clamped for 25 min immediately after right nephrectomy (Figure 1A). Mice received 5 μg of EVs or phosphate-buffered saline (PBS) (as a control) intravenously via the caudal vein immediately after reperfusion. A sham operation was also performed without clamping the renal vessel. The mice were killed 24 h after the operation. We observed a significant rise in the serum creatinine level in the IRI + PBS group, but a decrease in the serum creatinine level in the IRI + EV treatment group (Figure 1B), suggesting that MSC-EVs have a therapeutic effect on renal function. Terminal deoxynucleotidyl transferase-mediated d-UTP nick-end labeling (TUNEL) staining of kidney samples was performed to evaluate the apoptosis of renal cells, which is a critical pathophysiological event in AKI. MSC-EV administration significantly reduced TUNEL-positive cells, indicating the alleviation of renal cell apoptosis (Figure 1C). Histopathological examination revealed that tissue morphological and pathological changes were significantly attenuated in the IRI + EV treatment group compared with the IRI + PBS treatment group. The IRI + PBS group showed significant necrosis of renal tubular epithelial cells and proteinuria cast, while the IRI + EV treatment group exhibited reduced damage (Figure 1D). These findings suggest that MSC-EVs have the potential to reduce tissue damage and alleviate apoptosis in the context of IR-induced renal injury.

Identification of the functional protein component in MSC-EVs by proteomics analysis

To better understand the proteins in MSC-EVs, the EVs of MSC and fibroblasts were extracted and analyzed by mass spectrometry. We identified 101 proteins unique to MSC and 12 proteins unique to fibroblasts, whereas 338 proteins were overlapping (Figure 2A). Kyoto Encyclopedia of Genes and Genomics (KEGG) pathway analysis (http://www.kegg.jp/kegg/pathway.html) showed enrichment of genes encoding specific proteins in MSC-EVs associated with metabolic pathways, biosynthesis of antibiotics, carbon metabolism, and oxidative phosphorylation (Figure 2B).

Furthermore, we analyzed the subcellular localization of specific proteins in MSC-EVs. The percentage of mitochondrial proteins among the protein candidates of EVs was higher than 35%. The top five locations corresponded to the mitochondria (36%), endoplasmic

phosphate-buffered saline (PBS) or green fluorescent protein (GFP)/mitochondrial protein superoxide dismutase 2 (SOD2) mRNA-LNP were administrated intravenously immediately after reperfusion. (B) Serum creatinine level 24 h after operation and treatment. Data are expressed as the mean ± standard error of the mean of 7–11 samples per group (Sham: n = 7, IRI + PBS: n = 11, IRI + EV: n = 11). (C) Terminal deoxynucleotidyl transferase-mediated d-UTP nick-end labeling (TUNEL) staining and TUNEL-positive cells rate of kidney samples 24 h after operation and treatment (magnification ×200, scale bars, 100 μm). Data are expressed as the mean ± standard error of the mean of the 7–11 samples per group (Sham: n = 7, IRI+PBS: n = 11, IRI+EV: n = 11). (D) Representative micrographs of renal hematoxylin-eosin (H&E) histology staining 24 h after operation and treatment. Black arrow indicates cell nuclei defluxion; green arrow indicates cellular debris and proteinuria cast (scale bars, 100 μm). Statistical significance was determined using Kruskal-Wallis H-test (for non-normal distribution data) or one-way ANOVA (for normal distribution data) (****$p < 0.0001$).

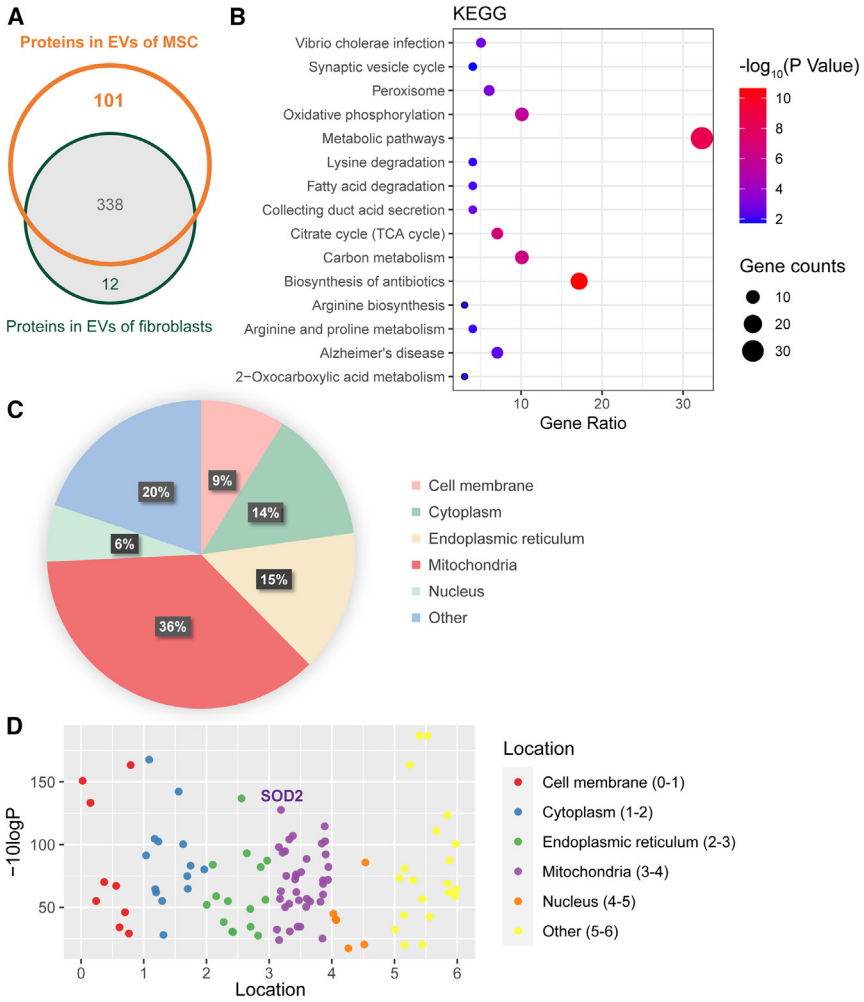

Figure 2. Proteomics analysis identified that SOD2 was enriched in MSC-EVs

(A) Venn diagram of proteins in the extracellular vesicles (EVs) of MSCs and fibroblasts. (B) KEGG pathway enrichment analysis for genes encoding the specific proteins in MSC-EVs. (C and D) Subcellular localization of specific proteins in MSC-EVs.

reticulum (15%), cytoplasm (14%), membrane (9%), and nucleus (6%). Therefore, we focused on mitochondrial proteins for further investigation (Figure 2C). The confidence score (−10logP) reflects how well the mass spectrometry results match the peptides for all observed mass spectrometry values that correspond to sequences within the protein. Therefore, protein ranking was performed based on the confidence score. The ranking revealed that SOD2 was one of the most abundant mitochondrial proteins (Figure 2D). In fact, in kidney IR, the mRNA level of *SOD2* was significantly lower in the tissue of kidneys with IRI than in the kidney tissue of the sham group (Figure S1C). Given the fact that SOD2 is an antioxidant enzyme, we hypothesized that supplementation with SOD2 protein may be a straightforward way to reduce oxidative stress in an IR-induced AKI model.

Chemically modified *SOD2* mRNA reduced mitochondrial ROS in HK-2 cells

To test this hypothesis, we synthesized HA-tagged *SOD2* mRNA as a protein replacement through *in vitro* transcription. The untranslated regions of the 5′ and 3′ terminals of mRNA were designed to enhance the translation efficiency of mRNA. To reduce the immunogenicity of IVT-mRNA, 5-Methoxy-UTP was used to replace regular UTP,[29,30] and mRNA was co-transcribed with the Cap1 analog.[31] The expression of *SOD2* mRNA was confirmed by both western blotting and immunofluorescence analysis in HeLa cells transfected with Lipofectamine 2000 (Figures S2A and S2B). Under a fluorescence microscope, SOD2-HA staining showed mitochondrial morphology, indicating physiological localization of the IVT-mRNA translated protein.

As naked mRNA is easily degraded by RNase in the circulatory system, we employed LNP encapsulation to extend its half-life and elicit efficient mRNA delivery *in vivo* (Figure 3A). mRNA was encapsulated in a lipid mixture composed of the ionizable cationic lipid SM102, cholesterol, DSPC, and DSPE-PEG2000 at a molar ratio of 50:38.5:10:1.5.[32] The encapsulation efficiency of green fluorescent protein (GFP) and *SOD2* mRNA-LNP was determined to be 90.47% and 91.43%, respectively, using a fluorescent RNA detection dye. Zeta potential analysis indicated that our LNPs had a negative zeta potential (GFP −2.016 ± 1.025 mV, SOD2 −4.009 ± 0.4778 mV) (Figure S2C). However, the surface charge was considered weak if the zeta potential falls between −20 and +20 mV.[33] Cryo-transmission electron microscopy images illustrated that *SOD2* mRNA-LNPs were spherical in shape (Figure 3B). The mRNA-LNPs were approximately 100 nm in diameter and had a polydispersity index less than 0.2, indicating good uniformity (Figure 3C). We first examined the cytosolic delivery of *SOD2* mRNA by LNP. After treatment of HK-2 cells with *GFP* or *SOD2* mRNA-LNP, we observed colocalization of SOD2-HA with mitochondria, as revealed by MitoTracker Deep Red (Figure 3D). The expression of *SOD2* mRNA-LNP was verified by real-time PCR, western blotting, and fluorescence, respectively (Figures 3E, S2D, and S2E). According to MitoSOX probing, we observed a significant decrease in mitochondrial superoxide anion levels, quantified after transfection with *SOD2* mRNA-LNP for 48 h when compared with *GFP* mRNA-LNP-treated cells (Figure 3F). Treatment of HK-2 cells with *SOD2* mRNA-LNP also suppressed intracellular ROS levels detected by both CellROX Green probe and H2DCFDA dye (Figures S2F and S2G). These results suggested that *SOD2*

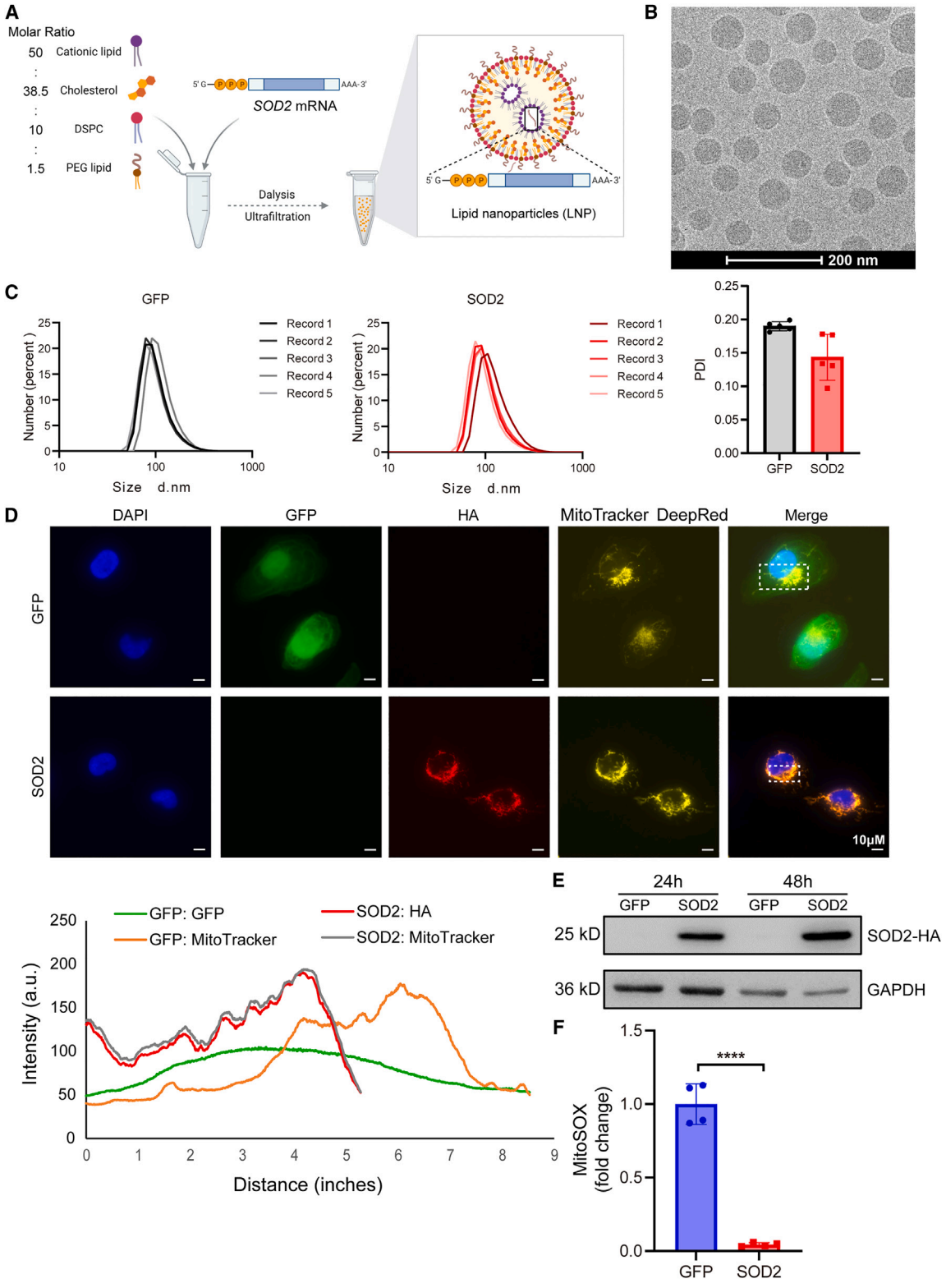

(legend on next page)

mRNA-LNP successfully expressed and overexpression of SOD2 exerted functions in HK-2 cells.

SOD2 mRNA-LNP reduced damage and acute renal dysfunction in the AKI model

To evaluate the therapeutic efficacy of *SOD2* mRNA in an IR-induced AKI model, we first examined the biodistribution of LNP delivered through different administration routes using firefly luciferase mRNA as a reporter. Because the mRNA-LNP mainly accumulated in the liver and spleen, when LNPs were administered through the caudal vein (Figure S3A), the luminescence signal was too weak in the renal region to be detected. Therefore, we applied renal subcapsular or intra-adipose capsule delivery of LNP in this study.

The two strategies showed similar delivery efficiencies revealed by similar bioluminescence intensities at 24 h. However, mRNA delivered through the renal capsule seemed to be expressed faster, as shown by higher bioluminescence intensity at 6 h. Renal capsule administration also exhibited a more precise targeting effect as bioluminescence signals were concentrated in the renal region (Figure 4A). The bioluminescent signals decayed over time. The signal of 48-h time point was significantly reduced to less than 20% of the signal at 24 h, then the signal of 72-h time point further decreased to less than 4% of the signal at 24 h (Figure S3B). Twenty-four hours after subcapsular or adipose capsule injection *ex vivo*, luminescence intensity was detected in various organs of mice, including the heart, liver, kidney, and spleen. Our findings indicated that the highest intensity of luminescence was observed in the kidney, compared with other organs. The results further revealed that renal capsule administration resulted in even higher luminescence intensity in the kidney (Figure S3C). Based on these findings, we ultimately selected renal capsule delivery of LNPs. Twelve hours after *SOD2* mRNA-LNP renal subcapsular injection, the expression of HA-tagged SOD2 was detected in tissues from the renal cortex and medulla regions after immunoprecipitation enrichment using anti-HA magnetic beads followed by western blotting (Figure 4B). The expression of *SOD2* mRNA-LNP in the kidney was also confirmed by real-time PCR (Figure S3D).

In the IR-induced AKI model, we found that the serum creatinine levels in the *SOD2* mRNA-LNP group were significantly lower than those in the *GFP* mRNA-LNP-treated group (Figure 4C). Moreover, *SOD2* mRNA-LNP treatment resulted in a significant decrease in blood urea nitrogen compared with both the *GFP* mRNA-LNP group and the IRI group (Figure 4D), suggesting that renal function was preserved after *SOD2* mRNA-LNP treatment. Histopathological analysis further showed that there was less disruption of the renal tubular structure and less bleeding in the IRI kidney tissue of mice treated with *SOD2* mRNA-LNP compared with the *GFP* mRNA-LNP treatment group (Figure 4E). IRI increased kidney weight and there was a minor decrease in body weight after surgery (Figures S3E and S3F).

To determine whether *SOD2* mRNA-LNP treatment exerted an antioxidative effect during AKI, the acquired kidney tissue samples were assayed for lipid oxidation. The assay involves the reaction of lipid peroxidation products, primarily malondialdehyde, with thiobarbituric acid, which results in the formation of the pink chromogen thiobarbituric acid reactive substance (TBARS). In our experimental study, it was observed that the kidney tissue of the IRI group and the IRI + *GFP* mRNA-LNP group exhibited a significant increase in TBARS content when compared with the Sham group. The kidney tissue of the IRI + *SOD2* mRNA-LNP group demonstrated a significantly lower TBARS content in comparison with both the IRI group and the IRI + *GFP* mRNA-LNP group. According to the results, lipid oxidation levels in the IRI + *SOD2* mRNA-LNP group were lower than those in the IRI + *GFP* mRNA-LNP group as well as the IRI group (Figure 4F). Furthermore, we measured tissue levels of 8-hydroxy-2′-deoxyguanosine (8-OHdG), which is a widely used indicator of oxidative DNA damage.[34] The results showed that the levels of 8-OHdG significantly decreased in the IRI + *SOD2* mRNA-LNP group compared with both the IRI + *GFP* mRNA-LNP group and the IRI group (Figure S3G).

In vivo biosafety of *SOD2* mRNA-LNP

To evaluate the *in vivo* side effects of mRNA-LNP, various organs were collected 24 h after mRNA-LNP treatment. We observed no histological differences in collected heart, lung, liver, or spleen tissues between the PBS-treated and mRNA-LNP-treated groups, suggesting no notable toxicity (Figure 5A). As kidney IR elicits acute liver injury,[35] we examined the plasma levels of alanine transaminase (ALT) and aspartate transaminase (AST) liver enzymes, which are released into the blood in higher levels when the liver is damaged. *SOD2* mRNA-LNP treatment seemed to protect against liver injury in mice with AKI, as indicated by a decrease in both AST and ALT levels compared with the control group (Figure 5B). Moreover, to investigate the immune response to *SOD2* mRNA-LNP, we measured the plasma levels of interleukin-6 (IL-6), which elicits pro-inflammatory properties in the AKI model. IL-6 levels in the serum were significantly increased in mice with AKI compared with those in the control group; however, no significant increase was observed in AKI mice with *SOD2* mRNA-LNP treatment compared with those in the AKI group (Figure 5C).

Figure 3. LNP delivery of chemically modified *SOD2* mRNA reduced ROS in HK-2 cells

(A) Scheme of lipid nanoparticle (LNP) packaging. DSPC, 1,2-distearoyl-sn-glycero-3-phosphocholine; PEG, polyethylene glycol. (B) Cryo-transmission electron microscopy image of *SOD2* mRNA-LNP (scale bar, 200 nm). (C) Size distribution and polydispersity index of LNP. (D) GFP, SOD2-HA (Alexa Fluor 568), and mitochondria were revealed by immunofluorescence and MitoTracker DeepRed staining, respectively, using fluorescence microscopy (scale bars, 10 μm). The quantification of colocalization between MitoTracker and GFP/SOD2-HA fluorescence was below the images. (E) Expression of SOD2-HA in HK-2 cells treated with 2 μg of *SOD2* mRNA-LNP for 24 h or 48 h determined by western blotting analysis. (F) MitoSOX Red staining and flow cytometry analysis of cells stained with MitoSOX dyes. Data are expressed as the mean ± standard error of the mean for four independent experiments. Statistical significance was determined using a Student's t test (n = 4, ****$p < 0.0001$).

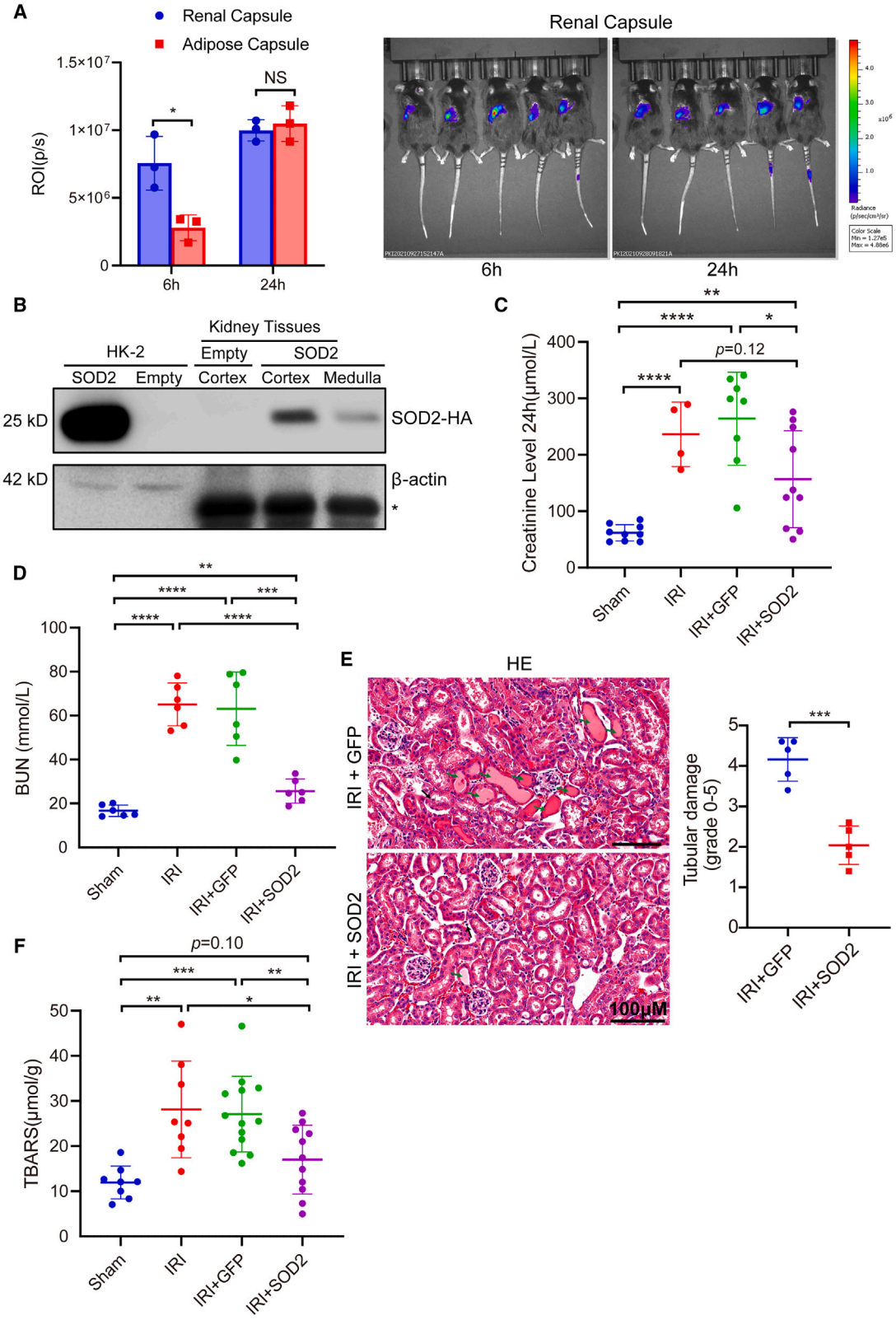

(legend on next page)

DISCUSSION

To dissect the mechanisms by which MSC-EVs confer protective effects in IR-induced AKI, we characterized the molecular composition of MSC-EVs in comparison with fibroblast-derived EVs by proteomic analysis. Our results revealed that mitochondrial components were enriched in EVs, with SOD2 being one of the most abundant proteins. Given that oxidative stress is deeply involved in IR-induced AKI, we assessed whether LNP delivery of the antioxidant enzyme *SOD2* mRNA could alleviate the course of IR-induced AKI. Our results showed that treatment with *SOD2* mRNA-LNP significantly attenuated IR-induced pathological injury in the kidney.

IR-induced AKI occurs under a variety of conditions, such as kidney transplantation, renal vascular occlusion, or obstruction, which interrupts the blood supply to the kidney.[36,37] As the pathophysiological mechanism of AKI is complex, it remains a key clinical challenge, with limited effective pharmacological methods available. Both stem cell therapy and stem cell-derived EVs have exhibited beneficial renoprotective effects, the latter of which exhibit greater stability, better biocompatibility, and lower immunogenicity than their source cells. As an important biocarrier, EVs mediate cell-cell communication by transferring cargo, such as proteins, lipids, and RNAs, into the target cells. Moreover, MSC-EVs can attenuate renal damage in a *cis*-platinum-induced AKI mouse model by reducing the expression levels of 8- hydroxy-2′ -deoxyguanosine, malonaldehyde, Bax, and caspase-3.[38] However, the underlying renoprotection mechanism of MSC-EVs in IR-induced AKI remains elusive. Previous research has shown that repair of mitochondrial functions is a crucial mechanism by which MSC-EVs mitigate IRI damage.[39,40] By employing comparative proteomics analysis, we identified the molecular components that contribute to this renoprotective effect. Specifically, we found that the proteins in EVs participate in various cellular processes, including metabolic pathways, antibiotic biosynthesis, carbon metabolism, and oxidative phosphorylation, which are associated with mitochondrial function. Moreover, most of the proteins in EVs were identified as mitochondrial proteins.

Multiple pathways exist for the uptake and release of EVs, including micropinocytosis, phagocytosis, endocytosis, and the direct fusion of EVs with the plasma membrane.[41] Although the mechanism by which EVs are secreted remains unknown, most cells constitutively secrete mitochondrial DNA and proteins in EVs.[42] Here, we showed that MSCs selectively package mitochondrial proteins into EVs under non-stimulated conditions and may transfer beneficial effects to the recipient cells. Among the protein candidates characterized by proteomics analysis, the mitochondrial protein SOD2 was identified as one of the most abundant. In mitochondria, SOD2 catalyzes the removal of superoxide radicals and the generation of oxygen and hydrogen peroxide, which can be further detoxified by catalase, glutathione peroxidase, or peroxiredoxins.[43] Superoxide dismutases are known to play protective roles in kidney injury including mitochondrial SOD (SOD2) and exocellular SOD (EC-SOD,SOD3).[44–46] Both SOD2 and catalase are downregulated during IR-induced AKI[47–49]; however, treatment with *SOD2* mRNA partially restored kidney function in this study. Moreover, the co-delivery of both *SOD2* mRNA and catalase mRNA may further enhance renoprotection in the IR-induced AKI model. The secretion of mitochondrial proteins may serve many functions, such as mitochondrial quality control, long-range metabolic modulation, immune regulation,[50] and recovery of the cellular function of damaged mitochondria.[51,52] Our study suggests that mitochondrial protein secretion may also affect the oxidative status of recipient cells and promote antioxidant protection, which could have important implications for IRI treatment.

During the reperfusion phase, which is accompanied by the release of cytokines and chemokines and the induction of inflammation, excessive amounts of ROS production affect mitochondrial oxidative phosphorylation and contribute to the functional deterioration of mitochondria, eventually leading to cell death. Therefore, targeting the delivery of therapeutic agents to mitochondria with antioxidative properties should be a highly effective treatment under conditions of oxidative stress, such as IRI.[53,54] In fact, several studies have shown the positive effects of antioxidants and ROS scavengers, such as EUK-134, a synthetic SOD/catalase mimetic,[55] picoliv,[56] resveratrol,[17] alpha-tocopherol,[18] naringin,[57] and aqueous garlic extract,[58] in combating IR-induced injury. Our results further highlight the effectiveness of antioxidants in protecting tissues from IR-induced damage. But, unlike some antioxidant chemicals that show toxicity and

Figure 4. Renal subcapsular administration of *SOD2* mRNA-LNP reduced ischemia-reperfusion-induced renal injury

(A) *In vivo* imaging at 6 h and 24 h after 0.5 mg/kg luciferase mRNA-LNP administration through the renal subcapsule. The scale of luminescence is indicated. Bar plots show a comparison of the total luminescence signal in the renal region. Region-of-interest (ROI) value is indicated in the renal region of mice subjected to subcapsular and adipose capsule injection. Small animal *in vivo* optical imaging was performed at two time points (6 h after injection and 24 h after injection). (B) Western blotting analysis was used to determine SOD2 expression by *SOD2* mRNA-LNP delivery in renal cells and tissues. *SOD2* mRNA-LNPs or empty LNPs were added to HK-2 cell culture media, or injected into the renal capsule. Four milligrams of total protein extracted from the renal cortex and medulla were incubated with HA magnetic beads to enrich SOD2-HA proteins. *Nonspecific band with HA antibody. (C) Serum creatinine level 24 h after operation and treatment. Quantitative data of serum creatinine were obtained from four to 10 samples in each group (Sham: n = 9, IRI: n = 4, IRI + GFP: n = 8, IRI + SOD2: n = 10). (D) Blood urea nitrogen (BUN) level 24 h after operation and treatment. Quantitative data of BUN were obtained from six samples in each group. (E) H&E staining of kidney samples 24 h after operation and treatment. Compared with mice treated with *GFP* mRNA-LNP, mice treated with *SOD2* mRNA-LNP showed less necrosis and bleeding (black arrow indicates cell nuclei defluxion; green arrow indicates cellular debris and proteinuria cast; scale bars, 100 μm). The histological injury score of kidney section after H&E staining was assessed by the sum total of these indicators: brush border loss 1′, Intratubular casts 2′, and tubular dilation 2′ (n = 5). (F) Lipid oxidation in kidney tissue measured by thiobarbituric acid reacting substances (TBARS) assay. Data are expressed as the mean ± standard error of the mean of the 8–13 samples per group (Sham: n = 8, IRI: n = 8, IRI + GFP: n = 13, IRI + SOD2: n = 11). Statistical significance was determined using Mann-Whitney test/Kruskal-Wallis H-test (for non-normal distribution data) or Student's t test/one-way ANOVA (for normal distribution data) (*$p < 0.05$, **$p < 0.01$, ***$p < 0.001$, ****$p < 0.0001$, NS, not significant).

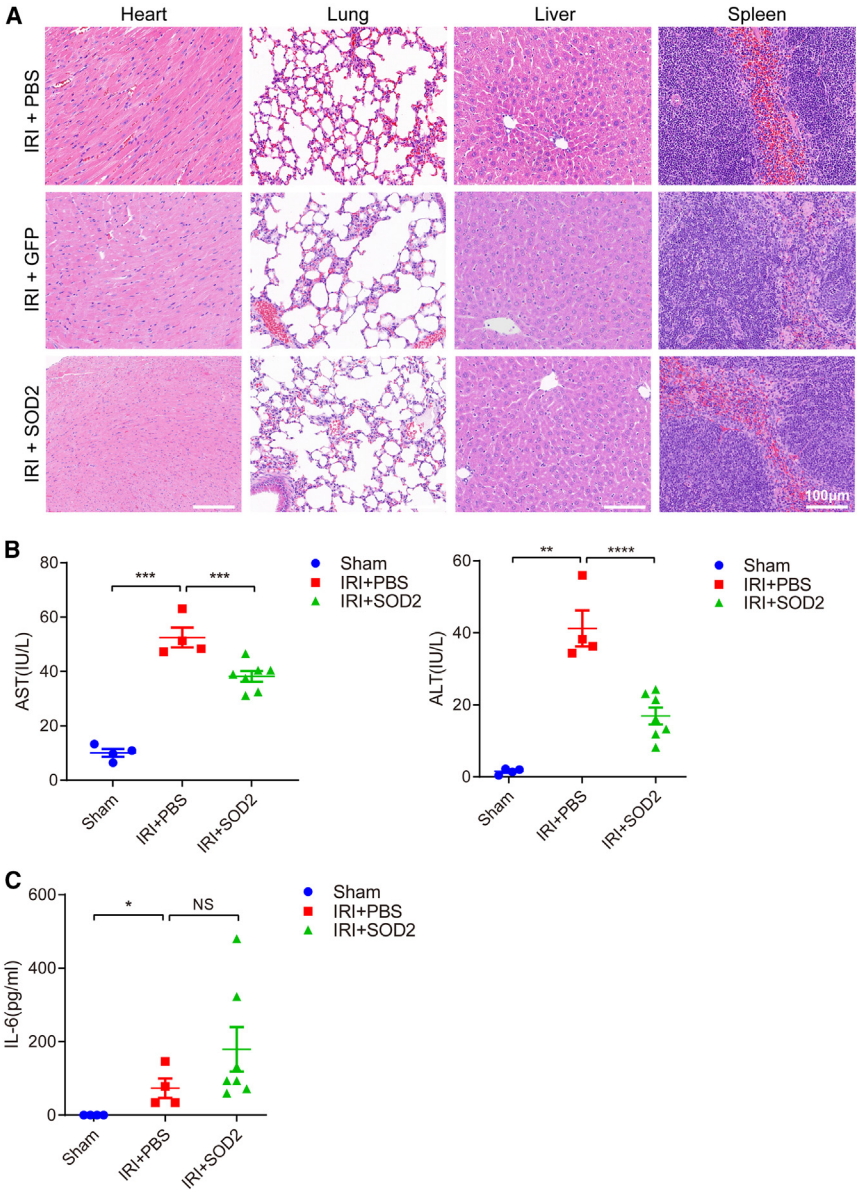

Figure 5. Safety profile of mRNA-LNP administration via the renal capsule in the ischemia-reperfusion-induced AKI model

(A) H&E staining of heart, lung, liver, and spleen sections from the PBS, *GFP* mRNA-LNP, and *SOD2* mRNA-LNP treatment groups in ischemia-reperfusion injury model mice (scale bars, 100 μm). (B) Serum aspartate transaminase (AST) and alanine transaminase (ALT) levels. (C) Serum interleukin-6 (IL-6) levels. Data are expressed as the mean ± standard error of the mean for the 4–7 samples per group (Sham: n = 4, IRI+PBS: n = 4, IRI+SOD2: n = 7). Statistical significance was determined using Kruskal-Wallis H-test (for non-normal distribution data) or one-way ANOVA (for normal distribution data) (*$p < 0.05$, **$p < 0.01$, ***$p < 0.001$, ****$p < 0.0001$, NS, not significant).

detrimental side effects,[59] host cell-produced SOD2 may elicit more physiological effects and have fewer safety concerns compared with new chemicals, as well as providing increased specificity toward ROS. In addition, mounting evidence highlights the beneficial effects of ROS under physiological conditions.[60,61] Universally suppressing ROS through small molecules can lead to profound consequences in organs that were not originally threatened by IRI. The local delivery of *SOD2* mRNA via LNP could enhance the organ specificity of antioxidant protection even further.

There are still some challenges that should be addressed before considering MSC-EVs as a therapeutic method for IR-induced AKI, such as the limited capacity for large-scale production, the heterogenicity of EVs, and the lack of stable isolation methods for ensuring the RNA and protein contents inside the EVs and ensuring their safety. LNP can serve as an alternative delivery platform for transferring renoprotective molecules when the critical beneficial components of EVs have been identified.

Moreover, the study has some limitations. First, we observed that *SOD2* mRNA expression in HK-2 cells reduced ROS levels; however, the mechanisms underlying the *in vivo* renoprotective effects of *SOD2* mRNA-LNP against IRI were not elucidated. Second, our study only examined the effect of SOD2, though other antioxidants such as catalase and GPX may also be of interest for future studies considering their potential role in mitigating oxidative stress generated by mitochondria in IRI. Third, our study is limited to the early stages of renal IRI (24 h) with a single dose. As a result, the long-term effects of IRI, such as fibrosis, and the effects of *SOD2* mRNA-LNP on these conditions remain uncertain. Our mRNA concentration in mRNA-LNP can reach up to ~500 ng/μL after concentration. However, local injection in the kidney capsule limited the volume of administration, and administering a volume greater than 10 μL would cause mRNA-LNP leakage. Therefore, we have chosen a dosing amount of 5 μg to ensure the maximum achievable dose under the current circumstances. The dose could be optimized in future studies. Finally, our study only focused on the role of oxidative stress. Hence, future research should also investigate the pathways involved in IR injury progression and the potential benefits of EVs, such as the nuclear factor-κB and transforming growth factor-β signaling pathways in hypoxia-induced renal fibrosis.[62–66]

MATERIALS AND METHODS

Ethics statement

All human participant research in this study was reviewed and approved by the Chinese Academy of Medical Science's institutional review board. This experiment was approved by the Research Ethics Committee at Shanghai Jiao Tong University First People's Hospital (Permit number 2013KY001).

Cell culture

Human renal proximal tubular cells (HK-2) from the Cell Bank of Shanghai Academy of Chinese Sciences were cultured in Dulbecco's Modified Eagle Medium/Nutrient mixture F-12 (DMEM/F-12) (BasalMedia) with 10% fetal bovine serum (FBS) (Gibco) under 5% CO_2 at 37°C. HeLa cells from ATCC were cultured with high-glucose DMEM (BasalMedia) with 10% FBS under 5% CO_2 at 37°C.

Preparation of cells and EVs

Human umbilical cords were collected from healthy term babies with the written consent of their parents and stored in Hank's balanced salt solution (Sigma-Aldrich) at 4°C. Human umbilical cord stem cells (MSCs) were obtained from Wharton's Jelly of the human umbilical cord as previously described.[67] The umbilical cords were selected based on the criteria of a healthy expectant mother (G1P0) with non-advanced maternal age, no complications during pregnancy, and a healthy full-term newborn delivered by cesarean. Briefly, human umbilical cords were cut into 1- to 2-mm^3 pieces and stuck to the bottom of cell culture plates in low-glucose DMEM (BasalMedia) with 10% FBS. Cells from the third to sixth passage were used in the experiments. Human fibroblasts were obtained from a commercial source (Shanghai Institute for Biological Sciences, Yueyang Road 320. Shanghai, China) and cultured in RPMI-1640 (Gibco) supplemented with 10% FBS.

EVs were isolated from MSCs and fibroblasts, as described previously.[68] Briefly, cells were cultured overnight in medium without FBS. The supernatant was collected on the second day. Conditioned medium was centrifuged at 2,000 × *g* for 20 min, filtered through 0.22-μm filters to remove cell debris, and further ultracentrifuged at 100,000 × *g* for 1 h at 4°C. The supernatant was removed and the EV pellet was resuspended in PBS. Subsequently, mesenchymal stem cell-derived extracellular vesicles (MSC-EVs) were used for experiments and frozen at −80°C for long-term storage.

Transmission electron microscopy of EVs

Transmission electron microscopy was performed at the Chinese Academy of Sciences Shanghai Branch and the Electron Microscopy Platform of Core Facility of Basic Medical Sciences, Shanghai Jiao Tong University School of Medicine. EVs were fixed with 2% paraformaldehyde for 5 min, loaded on a thin carbon film coated with 200-mesh copper grids, and allowed to stand for 5 min. The sample was the stained with a 1% uranyl acetate solution on the grids; excess solution was then removed using a filter paper. The samples were covered with a culture dish and dried for 10 min at room temperature, then observed using transmission electron microscopy (JEM-1230; Jeol, Japan) at 80 kV.

Western blotting analysis

Cells were homogenized in mammalian cell lysis buffer, then centrifuged at 13,000 × *g* for 20 min at 4°C. Protein concentration of whole-cell lysates or EVs was determined using the Bradford assay.[69] Equal amounts of protein were mixed with the sample loading buffer, boiled for 10 min, separated by SDS-PAGE under denaturing conditions, and electroblotted onto nitrocellulose membranes. Blotted membranes were blocked with 5% skim milk in Tris-buffered saline (pH 7.6)-0.2% Tween for 1 h. The proteins of interest were revealed with specific antibodies overnight at 4°C, followed by incubation with horseradish peroxidase-conjugated polyclonal anti-rabbit or anti-mouse immunoglobulin (Ig)G antibodies (1:10,000 dilution) for 1 h at room temperature. Antibody binding was detected using luminol-electrogenerated chemiluminescence (Tanon). CD63 (Abcam ab134045; 1:1,000 dilution), CD81 (Abcam ab109201; 1:1,000 dilution), Alix (CST 2171; 1:1,000 dilution), and TSG101 (Abcam ab125011; 1:1,000 dilution) antibodies were utilized as EV markers. HA (CST C29F4; 1:1,000 dilution), GAPDH (Proteintech 60004; 1:2,000 dilution), and β-actin (Proteintech 66009; 1:1,000 dilution) antibodies were utilized to determine SOD2-HA, GAPDH, and β-actin levels, respectively.

Animal model

Eight-week-old male C57BL/6J mice were purchased from the Animal Laboratory, Shanghai Jiaotong University School of Medicine, Shanghai, China. Female mice have been reported to exhibit higher resistance to IR treatment compared with male mice. IR treatment for 30 min resulted in a significant increase in serum creatinine levels in male mice, but not in female mice until 45 min, as reported by Park et al.[70] Due to this sex-based difference, male mice were selected for all experiments. All study protocols and animal care protocols were approved by the Animal Care and Experiment Committee of the Shanghai Jiaotong University School of Medicine (2019-097-01). All mice in this study were housed in microisolator cages with air circulation and free access to food and water. These cages were kept in a specific-pathogen-free room at an ambient temperature of 24°C with natural light and dark cycles. On the day of the operation, the mice were anesthetized using 3%–4% isoflurane for induction and 1%–2% isoflurane for maintenance. The total time under isoflurane anesthesia was approximately 40 min per experiment. After a midline laparotomy, the left renal pedicle was clamped for 25 min using an atraumatic vascular clamp to establish an ischemic AKI model, while the other side of the kidney was removed.[71] Mice in the sham group underwent laparotomy after anesthesia but no kidney IR was performed. To test the effect of MSC-EVs, 5 μg of EVs or only PBS control were administered by the caudal vein immediately after reperfusion. All mice were randomly divided into groups. The mice were killed 24 h after the operation, and the blood and kidney samples were collected and subjected to the following tests.

Renal function

Twenty-four hours after the operation, blood samples of the mice were collected in a vacutainer via cardiac puncture and allowed to stand for 60 min at 20°C, then centrifuged at 2,000 rpm for 15 min

to separate the serum. After removing protein from the serum, the serum creatinine was measured using a kit based on the Jaffe reaction (NJJCBIO). That is, in an alkaline environment, creatinine in the serum forms a creatinine-picrate complex by reacting with picrate. The absorbance of samples at 510 nm was measured and found to be directly proportional to the concentration of creatinine. The serum was also used to assess renal function by using a blood urea nitrogen detection kit (NJJCBIO) following the manufacturer's instructions.

Hematoxylin-eosin and TUNEL staining

Twenty-four hours after the operation, the kidney samples of the mice were collected and fixed in 4% paraformaldehyde, embedded in paraffin, and sectioned. The samples were then stained with hematoxylin-eosin (H&E) and the tubular damage was evaluated using the tubular damage score from the previous study.[72] The score is based on four indicators: brush border loss (1 score), tubular necrosis (1 score), intratubular casts (2 scores), and tubular dilation (2 scores). The sum of these scores is referred to as the tubular damage score. Five visual fields from one kidney cross-section were chosen and the average score was used to represent the kidney damage. To analyze cell apoptosis, terminal deoxynucleotidyl TUNEL staining was performed according to the manufacturer's instructions using the One-Step TUNEL Apoptosis Assay Kit (Beyotime). The TUNEL-positive cells were quantified using ImageJ.

Proteomics analysis of EVs

Ten millimolars of dithiothreitol was used to reduce MSC and fibroblast EV protein samples, which were then alkylated with 60 mM iodoacetamide. The samples were diluted with a solution of 100 mM triethylammonium bicarbonate, then digested with trypsin-LysC (Promega) for 16 h at 37°C. The samples were then pre-processed and injected into an LTQ-Orbitrap Fusion Mass Spectrometer (Thermo Fisher Scientific) coupled with an EASY-nLC 1000 Liquid Chromatograph Instrument (Thermo Fisher Scientific). Bioinformatics and statistical analyses of the original mass spectrometric data were performed using PEAKS Studio based on the UniProt database (20180524, 20349). Raw mass spectroscopy data were analyzed using PEAKS Studio version 8.5 (Bioinformatics Solutions, Waterloo, Canada) with 7 ppm MS and 0.05 Da MS/MS tolerances applied. The protein composition of EVs from MSC and fibroblasts was identified based on the results from PEAKS Studio. Our analysis found 101 unique proteins in MSC-EVs and 12 unique proteins in fibroblast EVs, with 338 proteins being overlapping. We then used Uniprot (https://www.uniprot.org/) to analyze the subcellular localization of the 101 specific proteins in MSC-EVs. The top five locations were the mitochondria (36%), endoplasmic reticulum (15%), cytoplasm (14%), membrane (9%), and nucleus (6%). As a result, we focused on mitochondrial proteins for further investigation. The confidence score (−10logP) calculated by PEAKS Studio measures how well the mass spectrometry results match the peptides for all observed mass spectrometry values that correspond to sequences within the protein. Protein ranking was performed based on the confidence score, revealing that mitochondrial protein superoxide dismutase 2 (SOD2) was one of the most abundant mitochondrial proteins.

Functional enrichment analysis

Protein localization was obtained from the UniProt database, and only primary localization of the proteins was used for the analysis. We used the R package "Clusterprofiler" for KEGG pathway analysis.[73] KEGG pathways with $p < 0.05$ were considered statistically significant.

In vitro transcription of *SOD2* mRNA

SOD2 mRNA was synthesized *in vitro* using a one-step T7 polymerase-mediated RNA transcription. Codon-optimized open reading frames with a C-terminal HA tag flanking the 5′ and 3′ untranslated regions (UTRs) were synthesized by General Biology (Anhui, China) and cloned into the downstream of T7 promoter of pcDNA3.1 vector. DNA templates containing the T7 promoter, coding sequence, UTRs, and a 100-bp poly(A-T) sequence at the 3′ end were amplified by PCR, purified, and used for *in vitro* transcription (IVT). The Cap1 analog (EzCap AG, APExBIO) was included in the IVT reaction to place a Cap1 structure at the 5′ end of the mRNA. mRNA was synthesized using regular nucleotides that were completely unmodified, except uridine (U) fully substituted with modified uridine analogs, 5-methyoxyuridine. Following transcription, the DNA template was removed using DNase I (New England BioLabs) at 37°C for 15 min mRNA was purified using RNA Clean & Concentrator Kits (Zymo Research).

Immunofluorescence staining

Cells were transiently transfected with GFP mRNA-LNP or *SOD2* mRNA-LNP. Twenty-four hours after transfection, the cells were plated on glass coverslips and cultured for an additional 24 h. Mitochondria were stained with MitoTracker DeepRed (Thermo Fisher Scientific) in the culture medium for 45 min followed by 1 h of recovery. The cells were then fixed with 4% paraformaldehyde for 30 min, treated with 0.2% Triton X-100 for 5 min, blocked with serum (2% normal goat serum and 2% bovine serum albumin) for 30 min, and stained with HA (CST C29F4; 1:200 dilution) antibody to detect SOD2-HA. The slides were washed and incubated with Alexa Fluor 568 goat anti-rabbit IgG (H + L) (Thermo Fisher Scientific). Nuclei were stained with 4′, 6-diamidino-2-phenylindole (DAPI; Sigma-Aldrich). Images were visualized under a fluorescence microscope (Leica DMi8; Leica Microsystems, Nussloch, Germany).

Detection of ROS

The mitochondrial production of O_2^- was determined using the mitochondrial superoxide indicator MitoSOX Red (Thermo Fisher Scientific). General oxidative stress indicator H2DCFDA (APExBIO) or CellROX Green Reagent (Thermo Fisher Scientific) was used to measure cellular ROS levels. Briefly, cells were incubated with 5 μM MitoSOX Red or 5 μM CellROX Green or 20 μM H2DCFDA for 30 min at 37°C in the dark. Cells stained with the dyes were analyzed by flow cytometry using a Beckman CytoFlex S flow cytometer.

Preparation of mRNA-loaded lipid nanoparticles

Lipids were dissolved in absolute ethanol at a molar ratio of 50:10:38.5:1.5 for DLin-MC3-DMA:DSPC:cholesterol:PEG2000-DMG. mRNA prepared with IVT was dissolved in 50 mM citrate

buffer by adding 1 M sodium citrate (pH 3.0) to prepare an acidic mRNA solution. Then, an equal volume of the lipid mixture and mRNA solution was mixed using a T-mixer. The formulations were immediately diluted 2-fold with 50 mM citrate buffer and dialyzed in PBS (pH 7.4) in Slide-A-Lyzer dialysis cassettes (Thermo Fisher Scientific) for at least 15 h. The formulations were passed through a 0.22-μm filter (Millipore) and concentrated using Amicon Ultra Centrifugal Filters (Millipore). RNA encapsulation for all formulations was measured using the Quant-iT RiboGreen RNA assay (Thermo Fischer Scientific). Particle sizes and zeta potential of LNPs were determined using a nanoparticle tracking analysis instrument (Zetasizer Nano ZS, Malvern).

Cryo-transmission electron microscopy sample preparation and imaging

Four microliters of concentrated mRNA-LNP sample was applied to a freshly glow-discharged grid (R2/1 Cu, 300 mesh, Quantifoil), and the grid was frozen in liquid ethane using a Vitrobot Mark IV System (Thermo Fisher Scientific) with a blot time of 3 s at 100% humidity and 4°C. The sample was imaged using a Talos F200C G2 transmission electron microscope (Thermo Fisher Scientific) at 200 kV. The magnification was set to 36,000× with a pixel size of 5.75 Å to visualize the dimensions of the nanoparticle.

mRNA-LNP delivery *in vivo* through the renal subcapsule or adipose capsule

The mouse kidney IRI model was the same as that described above. Immediately after left renal blood reperfusion, 5 μg mRNA-LNP or PBS control was injected into the renal subcapsule or adipose capsule with a microinjector. The needle of the microinjector containing mRNA-LNP pierced the renal subcapsule at the dorsolateral side of the kidney and moved slowly along the outline of the kidney. The mRNA-LNP was injected slowly, and the syringe was slowly pulled out 30 s after injection.

In vivo optical imaging and analysis of tissue luminescence intensity

Ten C57BL/6J mice were divided into two groups, and LNPs carrying firefly luciferase mRNA (APExBIO) (0.5 mg/kg) were injected into the renal subcapsule or adipose capsule. Mice were intraperitoneally injected with 150 mg/kg of D-luciferin (PerkinElmer) at 6, 24, 48, and 72 h after LNP administration. Fifteen minutes after the injection of D-luciferin, the mice were imaged using IVIS Spectrum CT (128201, PerkinElmer). Luminescence values of the renal region were quantified using Living Image Software (PerkinElmer).

Ten C57BL/6J mice were killed 24 h after firefly luciferase mRNA-LNP injection, when organ tissue samples were collected and subjected to tissue luminescence intensity testing. Organ tissue samples were cleaned with ice-cold PBS, crushed into small pieces, and soaked in PBS in 24-well plates. D-Luciferin (15 mg/mL) was then added to the samples. The luminescence intensity was measured using a Synergy H1 microplate reader (BioTek, Winooski, VT, USA) after 10 min of incubation at room temperature. Then, organ tissue samples were collected and dried overnight. The samples were weighed to calculate the tissue luminescence intensity per mass.

Real-time PCR

Total RNA was isolated from samples using an RNA Purification Kit (EZBioscience). Then, 1.2 μg of total RNA was reverse transcribed into cDNAs using HiScript III RT SuperMix (Vazyme) according to the manufacturer's instructions. Real-time PCR was performed on a LightCycler480 system (Roche) using SYBR Green Master Mix (Yeasen). The primers m*sod2*-F:gtgaacaatctcaacgcca and m*sod2*-R:gatagcctccagcaactct were used in this study. The primers detecting both mouse and human SOD2 were *SOD2*-F:aggagaagtaccaggaggcgt and *SOD2*-R:aggtttgtccagaaaatgcta. *Gapdh* was used as the internal control gene. Relative gene expression data were analyzed using the $2^{-\Delta\Delta CT}$ method.

Immunoprecipitation of SOD2-HA from tissue

To detect *SOD2* mRNA-LNP expression in the kidney, 10 μg *SOD2* mRNA-LNP tagged with HA or an equal volume of empty LNPs was administrated via renal subcapsular injection. Twelve hours after injection, the mice were killed, and kidney tissues were separated into the renal cortex and medulla. Kidney tissues were lysed with radioimmunoprecipitation assay buffer, and the extracted proteins were incubated with HA magnetic beads (Thermo Fisher Scientific) for 6 h at 4°C. HA-tagged proteins were eluted from beads by incubation at 95°C with 1× SDS loading buffer for western blot detection.

TBARS assay

Thiobarbituric acid reacting substances (TBARS), which measures malondialdehyde, was performed with a TBARS assay kit (Absin) following the manufacturer's instructions.

8-OHdG measurement

To evaluate oxidative stress levels, 8-hydroxy-2′-deoxyguanosine (8-OHdG) was measured by ELISA using the ELISA kit for 8-OHdG (CUSABIO) following the manufacturer's instruction.

In vivo toxicity evaluation: Histology, serum enzymatic assay, and immune response

For histological examination, IRI model mice were killed and various organs (heart, lung, liver, and spleen) were collected 24 h after the delivery of LNPs. All organs were separated and fixed overnight in 4% paraformaldehyde (Sangon Biotech) at 4°C. The fixed organs were embedded in paraffin, sectioned, and stained with H&E according to routine protocols. For the serum enzymatic assay, serum ALT and AST levels were evaluated using a colorimetric assay (Elabscience). The immune response was evaluated by determining interleukin-6 (IL-6) levels, which were directly measured using a mouse IL-6 ELISA Kit (Beyotime) following the manufacturer's instructions.

Statistical analysis

Data are presented as the mean ± standard error of the mean unless otherwise indicated. Statistical analyses were performed using Prism

software (GraphPad). We evaluated the normality of data using Shapiro-Wilk test. For the data with $p > 0.05$, we used the Student's t test or one-way ANOVA to evaluate the statistical significance. For the data with $p < 0.05$ (non-normal distribution data), we use non-parametric test (Mann-Whitney test or Kruskal-Wallis H-test) to evaluate the statistical significance. Significance was defined as $p < 0.05$ (*), $p < 0.01$ (**), $p < 0.001$ (***), or $p < 0.0001$ (****).

DATA AND CODE AVAILABILITY

All data are available in the main text or the supplemental materials.

SUPPLEMENTAL INFORMATION

Supplemental information can be found online at https://doi.org/10.1016/j.omtn.2023.102067.

ACKNOWLEDGMENTS

This research is supported by National Natural Science Foundation of China grant (31871430), National Natural Science Foundation of China grant (81470919), Shanghai Jiao Tong University Fund for Key Foresight in Scientific and Technological Innovation grant (2019TPA10), Key Medical Specialty in Jiading District, Shanghai grant (2020-jdyxzdzk-03), and Scientific Research Project of Shanghai Jiading District Health Committee grant (2021-KY-09).
Our proteomics and mass spectrometry work was performed at the Proteomics Platform of Core Facility of Basic Medical Sciences, Shanghai Jiao Tong University School of Medicine (SJTU-SM). We thank all the members of Yang and Xu Labs for their insightful discussions.

AUTHOR CONTRIBUTIONS

Y.-J.X., W.Y., and Y.-J.Z. designed research. Y.-T.H., S.-H.L., J.X., Y.Z., and Y.-N.Y. conducted research. Y.-T.H., S.-H.L., J.X., and M.-S.H. analyzed data. Y.-N.Y. audited the experimental procedures of extracellular vesicles collection. The manuscript was written by Y.-T.H., S.-H.L., J.X., and Y.Z., and revised by Y.-J.X., W.Y., and Y.-J.Z.

DECLARATION OF INTERESTS

Authors declare no competing interests.

REFERENCES

1. Bonventre, J.V., and Weinberg, J.M. (2003). Recent advances in the pathophysiology of ischemic acute renal failure. J. Am. Soc. Nephrol. *14*, 2199–2210. https://doi.org/10.1097/01.asn.0000079785.13922.f6.

2. Lee, S.A., Cozzi, M., Bush, E.L., and Rabb, H. (2018). Distant Organ Dysfunction in Acute Kidney Injury: A Review. Am. J. Kidney Dis. *72*, 846–856. https://doi.org/10.1053/j.ajkd.2018.03.028.

3. Zhang, X., Agborbesong, E., and Li, X. (2021). The Role of Mitochondria in Acute Kidney Injury and Chronic Kidney Disease and Its Therapeutic Potential. Int. J. Mol. Sci. *22*, 11253. https://doi.org/10.3390/ijms222011253.

4. Bhatia, D., Capili, A., and Choi, M.E. (2020). Mitochondrial dysfunction in kidney injury, inflammation, and disease: Potential therapeutic approaches. Kidney Res. Clin. Pract. *39*, 244–258. https://doi.org/10.23876/j.krcp.20.082.

5. Raedschelders, K., Ansley, D.M., and Chen, D.D.Y. (2012). The cellular and molecular origin of reactive oxygen species generation during myocardial ischemia and reperfusion. Pharmacol. Ther. *133*, 230–255. https://doi.org/10.1016/j.pharmthera.2011.11.004.

6. Han, S.J., and Lee, H.T. (2019). Mechanisms and therapeutic targets of ischemic acute kidney injury. Kidney Res. Clin. Pract. *38*, 427–440. https://doi.org/10.23876/j.krcp.19.062.

7. Jang, H.R., and Rabb, H. (2009). The innate immune response in ischemic acute kidney injury. Clin. Immunol. *130*, 41–50. https://doi.org/10.1016/j.clim.2008.08.016.

8. Sharfuddin, A.A., and Molitoris, B.A. (2011). Pathophysiology of ischemic acute kidney injury. Nat. Rev. Nephrol. *7*, 189–200. https://doi.org/10.1038/nrneph.2011.16.

9. Arslan, F., Lai, R.C., Smeets, M.B., Akeroyd, L., Choo, A., Aguor, E.N.E., Timmers, L., van Rijen, H.V., Doevendans, P.A., Pasterkamp, G., et al. (2013). Mesenchymal stem cell-derived exosomes increase ATP levels, decrease oxidative stress and activate PI3K/Akt pathway to enhance myocardial viability and prevent adverse remodeling after myocardial ischemia/reperfusion injury. Stem Cell Res. *10*, 301–312. https://doi.org/10.1016/j.scr.2013.01.002.

10. Xin, H., Chopp, M., Shen, L.H., Zhang, R.L., Zhang, L., Zhang, Z.G., and Li, Y. (2013). Multipotent mesenchymal stromal cells decrease transforming growth factor beta1 expression in microglia/macrophages and down-regulate plasminogen activator inhibitor 1 expression in astrocytes after stroke. Neurosci. Lett. *542*, 81–86. https://doi.org/10.1016/j.neulet.2013.02.046.

11. Simpson, R.J., Lim, J.W., Moritz, R.L., and Mathivanan, S. (2009). Exosomes: proteomic insights and diagnostic potential. Expert Rev. Proteomics *6*, 267–283. https://doi.org/10.1586/epr.09.17.

12. Vidal, M., Sainte-Marie, J., Philippot, J.R., and Bienvenue, A. (1989). Asymmetric distribution of phospholipids in the membrane of vesicles released during *in vitro* maturation of guinea pig reticulocytes: evidence precluding a role for "aminophospholipid translocase". J. Cell. Physiol. *140*, 455–462. https://doi.org/10.1002/jcp.1041400308.

13. Valadi, H., Ekström, K., Bossios, A., Sjöstrand, M., Lee, J.J., and Lötvall, J.O. (2007). Exosome-mediated transfer of mRNAs and microRNAs is a novel mechanism of genetic exchange between cells. Nat. Cell Biol. *9*, 654–659. https://doi.org/10.1038/ncb1596.

14. Waldenström, A., Gennebäck, N., Hellman, U., and Ronquist, G. (2012). Cardiomyocyte microvesicles contain DNA/RNA and convey biological messages to target cells. PLoS One *7*, e34653. https://doi.org/10.1371/journal.pone.0034653.

15. Ludwig, N., Whiteside, T.L., and Reichert, T.E. (2019). Challenges in Exosome Isolation and Analysis in Health and Disease. Int. J. Mol. Sci. *20*, 4684. https://doi.org/10.3390/ijms20194684.

16. Zhao, M., Wang, Y., Li, L., Liu, S., Wang, C., Yuan, Y., Yang, G., Chen, Y., Cheng, J., Lu, Y., and Liu, J. (2021). Mitochondrial ROS promote mitochondrial dysfunction and inflammation in ischemic acute kidney injury by disrupting TFAM-mediated mtDNA maintenance. Theranostics *11*, 1845–1863. https://doi.org/10.7150/thno.50905.

17. Giovannini, L., Migliori, M., Longoni, B.M., Das, D.K., Bertelli, A.A., Panichi, V., Filippi, C., and Bertelli, A. (2001). Resveratrol, a polyphenol found in wine, reduces ischemia reperfusion injury in rat kidneys. J. Cardiovasc. Pharmacol. *37*, 262–270. https://doi.org/10.1097/00005344-200103000-00004.

18. Rhoden, E.L., Pereira-Lima, L., Telöken, C., Lucas, M.L., Belló-Klein, A., and Rhoden, C.R. (2001). Beneficial effect of alpha-tocopherol in renal ischemia-reperfusion in rats. Jpn. J. Pharmacol. *87*, 164–166. https://doi.org/10.1254/jjp.87.164.

19. Bayati, A., Källskog, O., and Wolgast, M. (1990). The long-term outcome of post-ischaemic acute renal failure in the rat. I. A functional study after treatment with SOD and sucrose. Acta Physiol. Scand. *138*, 25–33. https://doi.org/10.1111/j.1748-1716.1990.tb08809.x.

20. Baker, G.L., Corry, R.J., and Autor, A.P. (1985). Oxygen free radical induced damage in kidneys subjected to warm ischemia and reperfusion. Protective effect of superoxide dismutase. Ann. Surg. *202*, 628–641. https://doi.org/10.1097/00000658-198511000-00016.

21. Greenwald, R.A. (1990). Superoxide dismutase and catalase as therapeutic agents for human diseases a critical review. Free Radic. Biol. Med. *8*, 201–209. https://doi.org/10.1016/0891-5849(90)90092-w.

22. Singh, I., Gulati, S., Orak, J.K., and Singh, A.K. (1993). Expression of antioxidant enzymes in rat kidney during ischemia-reperfusion injury. Mol. Cell. Biochem. *125*, 97–104. https://doi.org/10.1007/BF00936438.

23. Sahin, U., Karikó, K., and Türeci, Ö. (2014). mRNA-based therapeutics–developing a new class of drugs. Nat. Rev. Drug Discov. *13*, 759–780. https://doi.org/10.1038/nrd4278.

24. Maruggi, G., Zhang, C., Li, J., Ulmer, J.B., and Yu, D. (2019). mRNA as a Transformative Technology for Vaccine Development to Control Infectious Diseases. Mol. Ther. *27*, 757–772. https://doi.org/10.1016/j.ymthe.2019.01.020.

25. Pardi, N., Hogan, M.J., Porter, F.W., and Weissman, D. (2018). mRNA vaccines - a new era in vaccinology. Nat. Rev. Drug Discov. *17*, 261–279. https://doi.org/10.1038/nrd.2017.243.

26. Zhang, C., Maruggi, G., Shan, H., and Li, J. (2019). Advances in mRNA Vaccines for Infectious Diseases. Front. Immunol. *10*, 594. https://doi.org/10.3389/fimmu.2019.00594.

27. Karikó, K., Buckstein, M., Ni, H., and Weissman, D. (2005). Suppression of RNA recognition by Toll-like receptors: the impact of nucleoside modification and the evolutionary origin of RNA. Immunity *23*, 165–175. https://doi.org/10.1016/j.immuni.2005.06.008.

28. Hou, X., Zaks, T., Langer, R., and Dong, Y. (2021). Author Correction: Lipid nanoparticles for mRNA delivery. Nat. Rev. Mater. *6*, 1078–1094. https://doi.org/10.1038/s41578-021-00400-1.

29. Vaidyanathan, S., Azizian, K.T., Haque, A.K.M.A., Henderson, J.M., Hendel, A., Shore, S., Antony, J.S., Hogrefe, R.I., Kormann, M.S.D., Porteus, M.H., and McCaffrey, A.P. (2018). Uridine Depletion and Chemical Modification Increase Cas9 mRNA Activity and Reduce Immunogenicity without HPLC Purification. Mol. Ther. Nucleic Acids *12*, 530–542. https://doi.org/10.1016/j.omtn.2018.06.010.

30. Li, B., Luo, X., and Dong, Y. (2016). Effects of Chemically Modified Messenger RNA on Protein Expression. Bioconjugate Chem. *27*, 849–853. https://doi.org/10.1021/acs.bioconjchem.6b00090.

31. Lu, J., Lu, G., Tan, S., Xia, J., Xiong, H., Yu, X., Qi, Q., Yu, X., Li, L., Yu, H., et al. (2020). A COVID-19 mRNA vaccine encoding SARS-CoV-2 virus-like particles induces a strong antiviral-like immune response in mice. Cell Res. *30*, 936–939. https://doi.org/10.1038/s41422-020-00392-7.

32. ClinicalTrials.gov (2020). Safety and immunogenicity study of 2019-nCoV vaccine (mRNA-1273) for prophylaxis of SARS-CoV-2 infection (COVID-19). https://clinicaltrials.gov/ct2/show/NCT04283461.

33. Eygeris, Y., Gupta, M., Kim, J., and Sahay, G. (2022). Chemistry of Lipid Nanoparticles for RNA Delivery. Acc. Chem. Res. *55*, 2–12. https://doi.org/10.1021/acs.accounts.1c00544.

34. Degan, P., Bonassi, S., De Caterina, M., Korkina, L.G., Pinto, L., Scopacasa, F., Zatterale, A., Calzone, R., and Pagano, G. (1995). In vivo accumulation of 8-hydroxy-2'-deoxyguanosine in DNA correlates with release of reactive oxygen species in Fanconi's anaemia families. Carcinogenesis *16*, 735–741. https://doi.org/10.1093/carcin/16.4.735.

35. Shang, Y., Madduma Hewage, S., Wijerathne, C.U.B., Siow, Y.L., Isaak, C.K., and O, K. (2020). Kidney Ischemia-Reperfusion Elicits Acute Liver Injury and Inflammatory Response. Front. Med. *7*, 201. https://doi.org/10.3389/fmed.2020.00201.

36. Thadhani, R., Pascual, M., and Bonventre, J.V. (1996). Acute renal failure. N. Engl. J. Med. *334*, 1448–1460. https://doi.org/10.1056/NEJM199605303342207.

37. Levey, A.S., and James, M.T. (2017). Acute Kidney Injury. Ann. Intern. Med. *167*, ITC66–ITC80. https://doi.org/10.7326/AITC201711070.

38. Zhou, Y., Xu, H., Xu, W., Wang, B., Wu, H., Tao, Y., Zhang, B., Wang, M., Mao, F., Yan, Y., et al. (2013). Exosomes released by human umbilical cord mesenchymal stem cells protect against cisplatin-induced renal oxidative stress and apoptosis *in vivo* and *in vitro*. Stem Cell Res. Ther. *4*, 34. https://doi.org/10.1186/scrt194.

39. Gu, D., Zou, X., Ju, G., Zhang, G., Bao, E., and Zhu, Y. (2016). Mesenchymal Stromal Cells Derived Extracellular Vesicles Ameliorate Acute Renal Ischemia Reperfusion Injury by Inhibition of Mitochondrial Fission through miR-30. Stem Cell. Int. *2016*, 2093940. https://doi.org/10.1155/2016/2093940.

40. Zhao, M., Liu, S., Wang, C., Wang, Y., Wan, M., Liu, F., Gong, M., Yuan, Y., Chen, Y., Cheng, J., et al. (2021). Mesenchymal Stem Cell-Derived Extracellular Vesicles Attenuate Mitochondrial Damage and Inflammation by Stabilizing Mitochondrial DNA. ACS Nano *15*, 1519–1538. https://doi.org/10.1021/acsnano.0c08947.

41. Zhang, Y., Tan, J., Miao, Y., and Zhang, Q. (2021). The effect of extracellular vesicles on the regulation of mitochondria under hypoxia. Cell Death Dis. *12*, 358. https://doi.org/10.1038/s41419-021-03640-9.

42. Kowal, J., Arras, G., Colombo, M., Jouve, M., Morath, J.P., Primdal-Bengtson, B., Dingli, F., Loew, D., Tkach, M., and Théry, C. (2016). Proteomic comparison defines novel markers to characterize heterogeneous populations of extracellular vesicle subtypes. Proc. Natl. Acad. Sci. USA *113*, E968–E977. https://doi.org/10.1073/pnas.1521230113.

43. Trachootham, D., Lu, W., Ogasawara, M.A., Nilsa, R.D.V., and Huang, P. (2008). Redox regulation of cell survival. Antioxidants Redox Signal. *10*, 1343–1374. https://doi.org/10.1089/ars.2007.1957.

44. Tan, R.J., Zhou, D., Xiao, L., Zhou, L., Li, Y., Bastacky, S.I., Oury, T.D., and Liu, Y. (2015). Extracellular Superoxide Dismutase Protects against Proteinuric Kidney Disease. J. Am. Soc. Nephrol. *26*, 2447–2459. https://doi.org/10.1681/ASN.2014060613.

45. Hong, Y.A., Lim, J.H., Kim, M.Y., Kim, Y., Park, H.S., Kim, H.W., Choi, B.S., Chang, Y.S., Kim, H.W., Kim, T.Y., and Park, C.W. (2018). Extracellular Superoxide Dismutase Attenuates Renal Oxidative Stress Through the Activation of Adenosine Monophosphate-Activated Protein Kinase in Diabetic Nephropathy. Antioxidants Redox Signal. *28*, 1543–1561. https://doi.org/10.1089/ars.2017.7207.

46. Schneider, M.P., Sullivan, J.C., Wach, P.F., Boesen, E.I., Yamamoto, T., Fukai, T., Harrison, D.G., Pollock, D.M., and Pollock, J.S. (2010). Protective role of extracellular superoxide dismutase in renal ischemia/reperfusion injury. Kidney Int. *78*, 374–381. https://doi.org/10.1038/ki.2010.141.

47. Qian, Y., Guo, X., Che, L., Guan, X., Wu, B., Lu, R., Zhu, M., Pang, H., Yan, Y., Ni, Z., and Gu, L. (2018). Klotho Reduces Necroptosis by Targeting Oxidative Stress Involved in Renal Ischemic-Reperfusion Injury. Cell. Physiol. Biochem. *45*, 2268–2282. https://doi.org/10.1159/000488172.

48. Ratliff, B.B., Abdulmahdi, W., Pawar, R., and Wolin, M.S. (2016). Oxidant Mechanisms in Renal Injury and Disease. Antioxidants Redox Signal. *25*, 119–146. https://doi.org/10.1089/ars.2016.6665.

49. Chiang, C.K., Loh, J.Z., Yang, T.H., Huang, K.T., Wu, C.T., Guan, S.S., Liu, S.H., and Hung, K.Y. (2020). Prevention of acute kidney injury by low intensity pulsed ultrasound via anti-inflammation and anti-apoptosis. Sci. Rep. *10*, 14317. https://doi.org/10.1038/s41598-020-71330-1.

50. Todkar, K., Chikhi, L., Desjardins, V., El-Mortada, F., Pépin, G., and Germain, M. (2021). Selective packaging of mitochondrial proteins into extracellular vesicles prevents the release of mitochondrial DAMPs. Nat. Commun. *12*, 1971. https://doi.org/10.1038/s41467-021-21984-w.

51. Nargund, A.M., Pellegrino, M.W., Fiorese, C.J., Baker, B.M., and Haynes, C.M. (2012). Mitochondrial import efficiency of ATFS-1 regulates mitochondrial UPR activation. Science *337*, 587–590. https://doi.org/10.1126/science.1223560.

52. Calabria, E., Scambi, I., Bonafede, R., Schiaffino, L., Peroni, D., Potrich, V., Capelli, C., Schena, F., and Mariotti, R. (2019). ASCs-Exosomes Recover Coupling Efficiency and Mitochondrial Membrane Potential in an *in vitro* Model of ALS. Front. Neurosci. *13*, 1070. https://doi.org/10.3389/fnins.2019.01070.

53. Plotnikov, E.Y., Kazachenko, A.V., Vyssokikh, M.Y., Vasileva, A.K., Tcvirkun, D.V., Isaev, N.K., Kirpatovsky, V.I., and Zorov, D.B. (2007). The role of mitochondria in oxidative and nitrosative stress during ischemia/reperfusion in the rat kidney. Kidney Int. *72*, 1493–1502. https://doi.org/10.1038/sj.ki.5002568.

54. Malek, M., and Nematbakhsh, M. (2015). Renal ischemia/reperfusion injury; from pathophysiology to treatment. J. Ren. Inj. Prev. *4*, 20–27. https://doi.org/10.12861/jrip.2015.06.

55. Baker, K., Marcus, C.B., Huffman, K., Kruk, H., Malfroy, B., and Doctrow, S.R. (1998). Synthetic combined superoxide dismutase/catalase mimetics are protective as a delayed treatment in a rat stroke model: a key role for reactive oxygen species in ischemic brain injury. J. Pharmacol. Exp. Therapeut. *284*, 215–221.

56. Seth, P., Kumari, R., Madhavan, S., Singh, A.K., Mani, H., Banaudha, K.K., Sharma, S.C., Kulshreshtha, D.K., and Maheshwari, R.K. (2000). Prevention of renal ischemia–reperfusion-induced injury in rats by picroliv. Biochem. Pharmacol. *59*, 1315–1322. https://doi.org/10.1016/s0006-2952(00)00268-9.

57. Singh, D., and Chopra, K. (2004). The effect of naringin, a bioflavonoid on ischemia-reperfusion induced renal injury in rats. Pharmacol. Res. *50*, 187–193. https://doi.org/10.1016/j.phrs.2004.01.007.

58. Kabasakal, L., Sehirli, O., Cetinel, S., Cikler, E., Gedik, N., and Sener, G. (2005). Protective effect of aqueous garlic extract against renal ischemia/reperfusion injury in rats. J. Med. Food *8*, 319–326. https://doi.org/10.1089/jmf.2005.8.319.

59. Allison, S.J. (2012). Basic research: Kidney-specific antioxidant targeting for renal ischemic injury. Nat. Rev. Nephrol. *8*, 194. https://doi.org/10.1038/nrneph.2012.31.

60. Shadel, G.S., and Horvath, T.L. (2015). Mitochondrial ROS signaling in organismal homeostasis. Cell *163*, 560–569. https://doi.org/10.1016/j.cell.2015.10.001.

61. Sena, L.A., and Chandel, N.S. (2012). Physiological roles of mitochondrial reactive oxygen species. Mol. Cell *48*, 158–167. https://doi.org/10.1016/j.molcel.2012.09.025.

62. Kim, S., Lee, S.A., Yoon, H., Kim, M.Y., Yoo, J.K., Ahn, S.H., Park, C.H., Park, J., Nam, B.Y., Park, J.T., et al. (2021). Exosome-based delivery of super-repressor IkappaBalpha ameliorates kidney ischemia-reperfusion injury. Kidney Int. *100*, 570–584. https://doi.org/10.1016/j.kint.2021.04.039.

63. Lee, S.A., and Yoo, T.H. (2022). Therapeutic application of extracellular vesicles for various kidney diseases: a brief review. BMB Rep. *55*, 3–10. https://doi.org/10.5483/BMBRep.2022.55.1.141.

64. Tang, T.T., Wang, B., Wu, M., Li, Z.L., Feng, Y., Cao, J.Y., Yin, D., Liu, H., Tang, R.N., Crowley, S.D., et al. (2020). Extracellular vesicle-encapsulated IL-10 as novel nanotherapeutics against ischemic AKI. Sci. Adv. *6*, eaaz0748. https://doi.org/10.1126/sciadv.aaz0748.

65. Hertlein, V., Flores-Romero, H., Das, K.K., Fischer, S., Heunemann, M., Calleja-Felipe, M., Knafo, S., Hipp, K., Harter, K., Fitzgerald, J.C., and García-Sáez, A.J. (2020). MERLIN: a novel BRET-based proximity biosensor for studying mitochondria-ER contact sites. Life Sci. Alliance *3*, e201900600. https://doi.org/10.26508/lsa.201900600.

66. Lu, Y., Wang, L., Zhang, M., and Chen, Z. (2022). Mesenchymal Stem Cell-Derived Small Extracellular Vesicles: A Novel Approach for Kidney Disease Treatment. Int. J. Nanomed. *17*, 3603–3618. https://doi.org/10.2147/IJN.S372254.

67. Du, T., Cheng, J., Zhong, L., Zhao, X.F., Zhu, J., Zhu, Y.J., and Liu, G.H. (2012). The alleviation of acute and chronic kidney injury by human Wharton's jelly-derived mesenchymal stromal cells triggered by ischemia-reperfusion injury via an endocrine mechanism. Cytotherapy *14*, 1215–1227. https://doi.org/10.3109/14653249.2012.711471.

68. Zou, X., Gu, D., Zhang, G., Zhong, L., Cheng, Z., Liu, G., and Zhu, Y. (2016). NK Cell Regulatory Property is Involved in the Protective Role of MSC-Derived Extracellular Vesicles in Renal Ischemic Reperfusion Injury. Hum. Gene Ther. *27*, 926–935. https://doi.org/10.1089/hum.2016.057.

69. Bradford, M.M. (1976). A rapid and sensitive method for the quantitation of microgram quantities of protein utilizing the principle of protein-dye binding. Anal. Biochem. *72*, 248–254. https://doi.org/10.1006/abio.1976.9999.

70. Park, K.M., Kim, J.I., Ahn, Y., Bonventre, A.J., and Bonventre, J.V. (2004). Testosterone is responsible for enhanced susceptibility of males to ischemic renal injury. J. Biol. Chem. *279*, 52282–52292. https://doi.org/10.1074/jbc.M407629200.

71. Hesketh, E.E., Czopek, A., Clay, M., Borthwick, G., Ferenbach, D., Kluth, D., and Hughes, J. (2014). Renal ischaemia reperfusion injury: a mouse model of injury and regeneration. J. Vis. Exp. 51816. https://doi.org/10.3791/51816.

72. Yuan, X., Li, D., Chen, X., Han, C., Xu, L., Huang, T., Dong, Z., and Zhang, M. (2017). Extracellular vesicles from human-induced pluripotent stem cell-derived mesenchymal stromal cells (hiPSC-MSCs) protect against renal ischemia/reperfusion injury via delivering specificity protein (SP1) and transcriptional activating of sphingosine kinase 1 and inhibiting necroptosis. Cell Death Dis. *8*, 3200. https://doi.org/10.1038/s41419-017-0041-4.

73. Yu, G., Wang, L.G., Han, Y., and He, Q.Y. (2012). clusterProfiler: an R package for comparing biological themes among gene clusters. OMICS *16*, 284–287. https://doi.org/10.1089/omi.2011.0118.